Empirical correction of thermal responses in the Solar Occultation for Ice Experiment nitric oxide measurements and initial data validation results

David Gómez-Ramírez,[1,*] John W. C. McNabb,[1] James M. Russell III,[1] Mark E. Hervig,[2] Lance E. Deaver,[3] Greg Paxton,[3] and Peter F. Bernath[4]

[1]Department of Atmospheric and Planetary Sciences, Hampton University, 23 Tyler Street, Hampton, Virginia 23668, USA

[2]GATS Inc., 65 S Main St 5, Driggs, Idaho 83422, USA

[3]GATS Inc., 11864 Canon Blvd., Suite 101, Newport News, Virginia 23606, USA

[4]Department of Chemistry and Biochemistry, Old Dominion University, 4541 Hampton Blvd., Norfolk, Virginia 23529, USA

*Corresponding author: gomezd@vt.edu

Received 21 August 2012; revised 5 March 2013; accepted 29 March 2013;
posted 1 April 2013 (Doc. ID 174642); published 22 April 2013

The Solar Occultation for Ice Experiment (SOFIE) makes broadband transmission measurements centered at 5.32 μm to determine the concentration profile of nitric oxide (NO). These measurements show a signal oscillation due to detector temperature variations that severely limit the accuracy of NO retrievals if corrections are not applied. An empirical correction was developed to remove this instrumental error. This paper describes the correction, its impact on the retrieval, and presents a comparison from 87 to 105 km versus coincident atmospheric chemistry experiment—Fourier transform spectrometer (ACE-FTS) measurements. The southern hemisphere (SH) shows excellent agreement between the datasets, with statistically insignificant differences. The northern hemisphere (NH) SOFIE measurements exhibit a low bias of −18.5% compared to ACE-FTS. NH measurements (sunrise observations) are still under study, and only SH NO data (sunset observations) are currently publicly available as of SOFIE data version 1.2.

OCIS codes: (010.0280) Remote sensing and sensors; (120.6810) Thermal effects; (010.1280) Atmospheric composition.

http://dx.doi.org/10.1364/AO.52.002950

1. Introduction

Measurements of mesospheric nitric oxide (NO) are critical to understand the link between variations in the solar and geomagnetic environment of the Earth and its atmosphere. Generally, NO is produced in the mesosphere and thermosphere by solar soft x rays and extreme ultraviolet radiation. At polar latitudes however, auroral activity and energetic particle precipitation (EPP) during geomagnetic storm events drives the production of NO [1,2]. NO measurements are therefore important to characterize the effects of EPP and high-frequency radiation in the upper atmosphere. NO in the mesosphere and lower thermosphere (MLT) region can also be transported to lower altitudes where it participates in the catalytic destruction of stratospheric ozone, as documented by [3–5] among others. NO is also relevant for understanding the energy balance and radiative cooling of the upper atmosphere [6]. Currently, few satellite instruments in addition to the Solar Occultation for Ice Experiment (SOFIE) [7] routinely derive MLT NO concentrations from orbit. Independent

1559-128X/13/132950-10$15.00/0

NO measurements are available from the Atmospheric Chemistry Experiment—Fourier Transform Spectrometer (ACE-FTS) [8,9] which provide a similar vertical resolution and measurement geometry. Other satellite instruments that derive MLT NO concentrations are the Optical Spectrograph and Infrared Imaging System and the Sub-millimetre and Millimetre Radiometer [10,11] on board the Odin satellite and, until April 2012, the Michelson Interferometer for Passive Atmospheric Sounding [12] and the Scanning Imaging Absorption Spectrometer for Atmospheric Chartography [13] from the European Space Agency's Environmental Satellite.

The SOFIE instrument, on board the aeronomy of ice in the mesosphere (AIM) satellite [14], uses solar occultation and differential broadband radiometry to measure the vertical profiles of temperature, polar mesospheric cloud extinction, aerosols, and several gas constituents of the middle atmosphere, including water vapor (H_2O), ozone (O_3), methane (CH_4), carbon dioxide (CO_2), and NO. Measurements are performed in a total of 16 spectral bands, organized by pairs into eight channels with center wavelengths extending from 0.29 to 5.32 μm. The basic measurement approach is to ratio the signal in the various channels obtained while viewing the sun through the atmospheric limb to the signal obtained while viewing above the sensible atmosphere. Thermoelectric coolers (TECs) are coupled to every detector to maintain a constant temperature and minimize thermally induced signal changes. To monitor the thermal behavior of each band, the instrument is also equipped with temperature sensors on each detector. As the spacecraft experiences sunrise or sunset, changes in the energy reaching the instrument cause the detectors to heat or cool. The design of the control circuitry for the TECs results in small oscillations of the detector temperature during the occultation event, until the TECs reach a steady state temperature. These oscillations are only significant in the broadband NO channel.

Channel eight in the instrument was specifically tailored to measure NO using broadband extinction measurements centered at 5.32 μm. After launch, the 5.32 μm band detector signal showed an unexpected temperature response that compromised the accuracy of the NO retrieval. The present paper describes the solution implemented to restore the quality of the SOFIE NO data. To verify that the resulting NO retrieval from the corrected transmission signals is accurate, a comparison was made with concurrent NO measurements by the ACE-FTS instrument. The ACE-FTS retrieved NO values have been validated for the stratosphere and lower mesosphere [15], providing a good database for assessing the quality of SOFIE measurements. This paper describes the state of the SOFIE NO retrievals as of dataset version 1.2.

2. Modeling the Detector Thermal Response

The SOFIE instrument performs measurements in two different modes, i.e., spacecraft sunset (SS) and spacecraft sunrise (SR). The SS mode refers to the solar occultation measurement performed when the AIM satellite is in the ascending portion of the orbit, but before crossing the equatorial plane. The sunset mode measurements occur exclusively in the southern hemisphere (SH). On the other hand, the SR mode also occurs in the ascending portion of the orbit, but after crossing the equatorial plane, restricting these events to the northern hemisphere (NH). The distinction is important because the thermal shock experienced by the instrument, and the subsequent oscillation in the transmission signal, are different for each spacecraft mode.

During SS measurements, the detectors within the instrument first receive the solar energy input when pointing at a high tangent altitude of ~300 km. Actual operational measurements do not begin until the tangent altitude is 180 km, about 60 s afterward. At this point in time, the oscillation has been dampened and is small for most events. During SR, however, the thermal shock and data collection occur simultaneously as the satellite emerges from the dark side of the planet, when the tangent altitude is 0 km. Examples of the behavior of the 5.32 μm transmission signal for the two different modes are depicted in panel (a) of Figs. 1 and 2. The altitude in these figures refers to the geodetic altitude, determined from orbital ephemeris and instrument pointing.

The corresponding detector temperatures for the example events are shown in panel (b) of Figs. 1 and 2. It is clear that the signal variations in the sunrise event anticorrelate strongly with the changes in the temperature of the detector. The combination of the coarse time resolution and noise in the measured detector temperatures makes it difficult to qualitatively distinguish the oscillation in the detector temperature for the sunset events. The coarse time resolution of the temperatures also prevents an accurate characterization of the thermal response of the detector. For this reason, the thermal response is analyzed based on the actual transmission measurement in the 5.32 μm band.

The thermal oscillation in the transmission signal, M_{osc}, is accurately modeled by an exponentially decaying sinusoidal wave as shown by Eq. (1):

$$M_{\mathrm{osc}} = A\left[\exp\left(-\frac{\Delta t}{\tau}\right)\sin(\omega\Delta t + \phi) - \sin(\phi)\right] + S\Delta t, \tag{1}$$

where A is the amplitude and ϕ the phase of the oscillation. τ is a decay constant, and ω refers to the frequency of the oscillation. The transmission signals show a linearly increasing value at exoatmospheric altitudes, where no atmospheric signal is present. This characteristic of the measurement, possibly also related to the thermal stability of the instrument, is corrected with the term S, which models the linear drift in the signal. The model is a function of Δt, defined as the time difference between the time of the measurement (t_m) and a reference time (t_0), taken

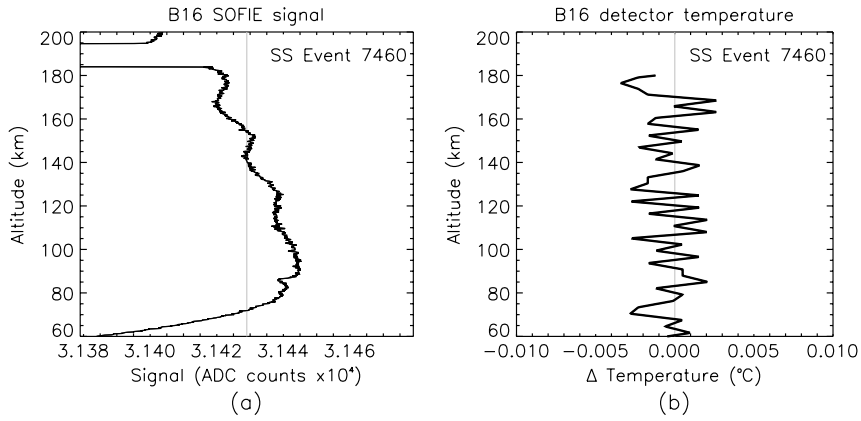

Fig. 1. (a) Oscillation in the SOFIE 5.32 μm signal during a SS measurement. (b) Corresponding oscillation in the detector temperature for that same event.

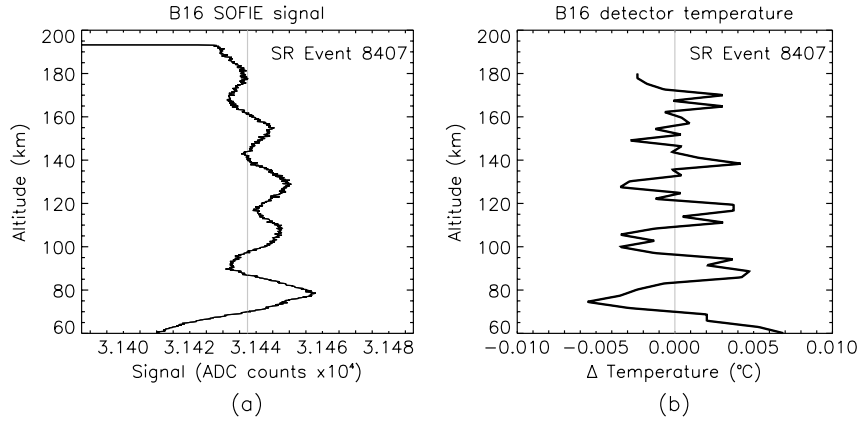

Fig. 2. (a) Oscillation in the SOFIE 5.32 μm signal during a SR measurement. (b) Corresponding oscillation in the detector temperature for that same event.

when the tangent altitude is 140 km. The altitude of 140 km was chosen to be the initial boundary of the sensible atmosphere, based on experience with the data. The constant term $-\sin(\phi)$ sets the initial condition that M_{osc} at t_0 is equal to zero. Figures 1 and 2 confirm the oscillatory nature of the data and show that the removal of the oscillation is needed for both the sunset and sunrise modes. It is especially critical for sunrise events because the amplitude of the oscillation increases exponentially at lower tangent altitudes. The oscillatory correction for the sunset mode is smaller and, contrary to the sunrise mode, the amplitude of the oscillation decays exponentially at lower altitudes. However, the sunset signals must still be corrected for the linear drift in the measurement, which cannot be accurately determined without correctly accounting for the thermal oscillation.

To correctly apply the oscillation model to the measured signal, a gain related to an instrumental calibration procedure called balance adjustment (BA) must be taken into account. The BA procedure introduces a sharp step in the signal level between 180 and 200 km. The time of occurrence and duration of this calibration procedure changes slightly from event-to-event. The BA procedure modifies the electronic gain applied to the measured signal with the objective of optimizing the observation. The gain, C_{BA}, changes before and after the BA (defined by the time t_{BA}), as expressed in Eq. (2). C_{pre} and C_{post} are the gains before and after the BA procedure, respectively, and $\theta(\Delta t)$ is a step function that sets the gains accordingly:

$$C_{\text{BA}} = C_{\text{pre}}\theta(\Delta t < t_{\text{BA}}) + C_{\text{post}}\theta(\Delta t > t_{\text{BA}}). \quad (2)$$

The exoatmospheric signal value V_0, is defined in the algorithm as the measured signal at 140 km. The oscillation must be modeled at the exoatmospheric level to correctly match the model and the signal. The model is thus offset by the exoatmospheric reference value and is modified as shown in Eq. (3):

$$M = V_0 C_{\text{BA}}(1 - M_{\text{osc}}). \quad (3)$$

This completes the model of the oscillation in the signal. The total number of fitting parameters is seven (the two BA gains and the five oscillation parameters A, ϕ, S, τ, and ω). The V_0 value and the t_{BA} are either calculated or provided to the algorithm

and are held as constants during the fit. Notice that, ideally, the exoatmospheric portion of the signal should be completely flat at $V_0 C_{\mathrm{BA}}$ based upon the fundamental assumption that the solar energy is not changing during the measurement. This portion of the signal is ideal for fitting the model for the correction since there is no actual atmospheric perturbation in the measurement. The decay and frequency of the oscillation were found to be approximately constant as described in Section 3.A, thus reducing the number of fitting parameters for a given event to five.

3. Thermal Response Removal Algorithm

A Levenberg–Marquardt (LM) algorithm [16] is used to perform a least-squares fit of the signal using the model described. The fit is only performed in the exoatmospheric altitude range, where no atmospheric signals are present. The fitted parameters for the exoatmospheric altitude range are used to extrapolate the model to cover the entire signal. The oscillation is then removed, and the exoatmospheric signal level is restored as described by Eq. (4), where V_m is the original measured signal and V_c is the corrected one. Notice that for Eq. (4), M refers to the extrapolation over the entire signal range:

$$V_c = V_m - M + V_0 C_{\mathrm{BA}} = V_m + M_{\mathrm{osc}} V_0 C_{\mathrm{BA}}. \quad (4)$$

The fundamental SOFIE measurement for the retrieval is the limb path transmission in the NO band. Extinction by atmospheric NO is then inferred using the ratio of the endoatmospheric to the exoatmospheric signal defined by Eq. (5):

$$\beta = 1 - \frac{V_c}{V_0}. \quad (5)$$

It is assumed that the limb path extinction cannot be negative, or equivalently the limb transmission cannot be greater than one, a feature that should be monitored in the corrected signal. If statistically significant unphysical negative extinctions are present in the corrected profile, it can be assumed that the correction failed.

The LM algorithm minimizes the χ^2 statistic, defined in Eq. (6), to arrive at the best fit solution. The term σ_i refers to the signal random noise, N is the number of fitted datapoints, and the subscript "fit" is used to signify that the χ^2 is only calculated for the fitted altitude range. Δ_{fit_i} is the difference between the signal and the model throughout the fitting range, $V_m(\Delta t_i) - M(\Delta t_i)$:

$$\chi^2 = \sum_{i=1}^{N} \frac{(\Delta_{\mathrm{fit}_i})^2}{\sigma_i^2}. \quad (6)$$

The reduced χ^2 (χ^2_{red}) was used as an alternative to assess the performance of the fitting routine. The χ^2_{red} corresponds to the ratio of the χ^2 to the number of degrees of freedom, ν, defined as $N - n - 1$, where N is the number of datapoints that are fitted, and n is the number of free parameters in the fit. Difficulties in implementing the fitting procedure occur because of the limited amount of data available for the fit. Additionally, the weak oscillations observed at the exoatmospheric altitudes limit the accuracy of the model parameterization.

To minimize the presence of unphysical negative extinctions in the corrected signal, a penalty was introduced to the fit. The penalty consists of increasing the differences used for convergence by the LM algorithm by an amount proportional to the total statistically significant unphysical values. The LM algorithm will therefore look for the combination of parameters that best minimizes both the unphysical signals and the thermal oscillation. To avoid overcorrecting, the penalty does not take into account those values that are below the 1σ error of the exoatmospheric reference.

The highest altitude at which the concentration of a constituent gas can be retrieved occurs where the response of the retrieved product to the expected transmission signal is at least 3 times the response to the instrumental noise. This altitude for SOFIE varies depending on absorption band and event from ~100 to ~140 km. The portion of the measurement above this limit is denoted as exoatmospheric, meaning that the effect of the atmosphere is not detectable. Below the 140–100 km mark, the signal is endoatmospheric and the measurements contain important information about the concentrations of the absorbing gases. When removing the thermal response of the 5.32 μm detector, a danger exists of removing part of the actual atmospheric signal. Therefore, it is crucial to identify the lowest altitude of the atmosphere that can be deemed exoatmospheric. A compromise must be reached, however, since the more data that are available for the fit, the better the detector thermal response can be determined and corrected. The challenge in adequately choosing the fitting range lies in identifying the altitude where the signal is entirely exoatmospheric. The algorithm starts at a predefined altitude of 140 km and increases the fitting range in 1 km increments until reaching a lower limit of 100 km. The best altitude range is selected according to the lowest χ^2_{red} statistic obtained from the fit. If there are additional features in the signal that are not described by the model, the χ^2_{red} statistic will increase, constraining the fitting region only to altitudes that can be fully explained by the thermal oscillation model. It is expected that atmospheric effects on the signal will not be in coincident phase with the model, and therefore will increase the χ^2_{red} statistic if they are included inside the fitting altitude range.

A. Characterization of the Detector Thermal Response

During May 2009, the SOFIE instrument was commanded to generate a set of 15 calibration measurements. These calibration events occurred exclusively

in the sunset mode above a tangent altitude of 180 km, to ensure that there were no atmospheric effects on the measured solar radiation signal. In operational events, this time is used to execute pointing procedures that characterize the solar source function for the different absorption bands, hence the calibration events are referred to as "no solar source function" (no-SSF) events. The no-SSF measurements provide an entirely exoatmospheric signal that most clearly shows the thermal oscillation for an extended time and altitude range. One of the calibration events is shown in Fig. 3. The data are plotted with respect to the time Δt used to fit the model. The additional exoatmospheric data provided by these special events includes all the measurements before −20 s (i.e., above ∼180 km). Operational events provide about 15 s of exoatmospheric measurements, whereas in no-SSF events, about 55 s of data are available for the fit. The model was fit to these calibration events, and the overall frequency and decay of the oscillation was found to be approximately constant. This result is in agreement with the thermal response being caused by the TEC control hardware configuration, which does not change from orbit to orbit.

Since the number of no-SSF events is limited to May of 2009, possible drifts in the constant decay and frequency were investigated by analyzing the detector temperature data. As previously noted, the precision and temporal resolution of the single event detector temperature data are not adequate, hence 15 event averages were calculated on a data sample every 15 days for the entire mission. Only the temperature data for the sunrise mode measurements were considered because the sunset temperature measurements are dominated by the noise in the temperature sensor. The average detector temperature profiles were then fitted with the model.

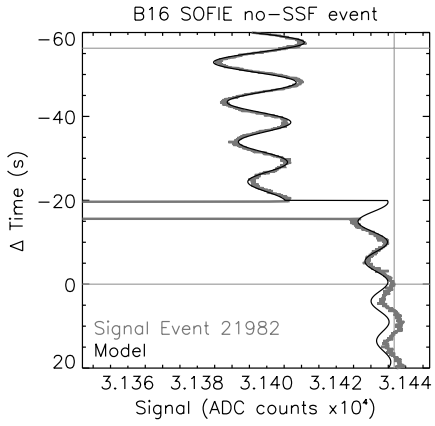

Fig. 3. Example of a "no solar source function" (no-SSF) calibration event taken during May 2009. The event is shown in gray and the model is shown in black. The vertical line corresponds to the exoatmospheric level defined as the signal value at $\Delta t = 0$, which corresponds to a tangent height of approximately 140 km. The horizontal lines indicate the range over which the signal data are being fitted. The BA caused the discontinuity from −15 to −20 s.

The data showed that the decay and frequency determined from the detector temperatures is within the uncertainties of the parameters calculated from the no-SSF events, providing further motivation to use a constant decay and frequency as calculated by the no-SSF events. The signal error from analog to digital converter (ADC) noise was also characterized using the no-SSF data and found to be 0.54 counts, which is consistent with the ADC theoretical error of 0.5 counts.

B. Uncertainty of the Absorption Signal

The uncertainty introduced into the signal by the correction is a combination of the uncertainty in the fitting parameters, the uncertainty incurred by fixing or not fixing the decay and frequency, and the uncertainty in the optimal fitting altitude range. To calculate the uncertainty caused by the fitting parameters, all possible combinations of the parameters with a ± 1 sigma error applied were considered. At each altitude, the maximum and minimum possible signal values are selected to form the extremum profiles according to the errors in the parameters.

Fixing the decay and the frequency also introduces some error if these parameters vary slightly from event to event. The frequency was found both in the no-SSF calibration events and the detector temperature data to vary negligibly (by less than 1%) and therefore this uncertainty is not calculated. The decay, on the other hand, has a standard deviation from the no-SSF calibration events of 7.7%, which can introduce significant variation to the signal profiles. The correction was applied with a variable decay to estimate the uncertainty introduced by fixing this value in the model.

The fitting range that yields the best χ^2_{red} is reported to calculate the NO retrieval. It was determined empirically that a χ^2_{red} smaller than 3.0 was acceptable. Hence the profile obtained using the longest fitting range that still returns a $\chi^2_{\mathrm{red}} < 3$ was used to estimate the uncertainty in the optimal fitting range. All uncertainties were considered independent of each other and are added in quadrature to yield the total uncertainty introduced by the thermal response correction to the detector signal.

C. Thermal Response Removal Statistics

The algorithm was tested using the SOFIE 2008 data to determine the performance of the thermal response correction. The correction algorithm returns two flags to identify the events that the algorithm failed to accurately fit. One flag is set if the χ^2_{red} is greater than the 3.0 threshold. The other flag is set if the unphysical value of the extinction, defined previously by Eq. (5), is lower than -1×10^{-4} (corresponding to a maximum of 3.3 ADC counts above the exoatmospheric value). A total of 9545 events were analyzed to verify the performance of the applied correction to the signal. 336 events (3.5%) had an unacceptable χ^2_{red}, and 256 (2.7%) still showed unphysical signals. 137 events (1.4%) showed both

flags, indicative that about half of the unphysical signals are the result of erroneous fits. The average χ^2_{red} for the accepted events was 1.60 with a standard deviation of 0.33. The lowest altitude for the fitting altitude range as described in Section 3 varies from 100 to 140 km. On average, the correction starts at an altitude of 128 km for the 2008 events. However, the correction starting point is biased to upper altitudes. The correction for 50.4% of the events starts above 130 km, and it starts below an altitude of 110 km for only 10.5% of the events corrected.

Examples of the 5.32 μm detector signal correction for a SS event and SR event are shown, respectively, in Figs. 4 and 5. Notice that the correction uncertainty in the sunset example is almost unnoticeable. The false signal oscillations in the sunset data have been completely removed. Sunrise events, because of the nature of the initial thermal shock, show greater uncertainties in the correction with decreasing altitude.

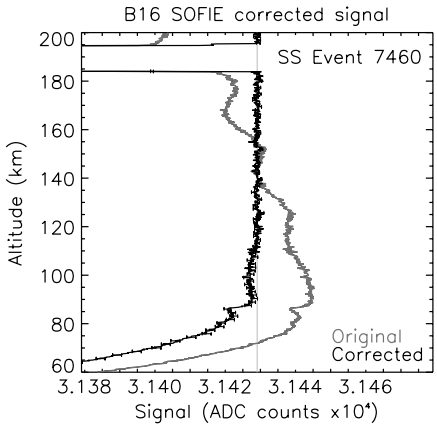

Fig. 4. Example of the correction applied to a sunset event. The original signal is shown in gray and the corrected signal in black along with its uncertainty.

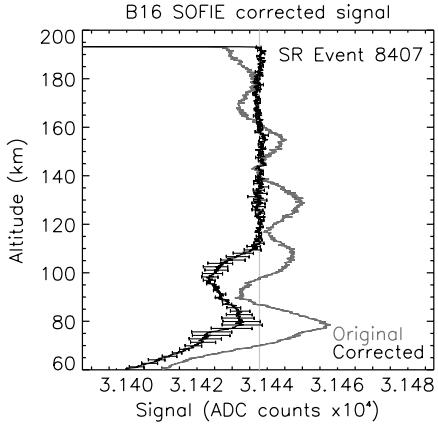

Fig. 5. Example of the correction applied to a sunrise event. The original signal is shown in gray and the corrected signal in black along with its uncertainty.

4. Nitric Oxide Retrieval

The retrieval of NO is performed using the 5.32 μm absorption band signal, with an "onion-peeling" algorithm [17]. A detailed description of the signal processing and data retrieval is given in [7]. To obtain the NO concentration for each Earth limb tangent layer, the transmission signal at each tangent altitude is iteratively simulated with different concentrations until the simulated transmission matches the measured transmission to within the noise level. In the operational retrieval, the signal profile is divided into seven independent profiles or interleaves to reduce random error, taking advantage of the high vertical sampling rate of SOFIE. The target gas is retrieved for each interleave and the retrievals from the seven interleaves are combined to generate the final retrieval product [7]. An important note is that the retrieval algorithm outputs a minimum volume mixing ratio (VMR) value of 1×10^{-15} parts per volume (ppv) (NO density of ~0.01 cm^{-3} at 100 km) when the signal-to-noise ratio (SNR) is not enough to derive the atmospheric constituent concentration. Further averaging in the retrieval algorithm leads to minimum NO VMRs of $\sim 1 \times 10^{-10}$ (densities of ~1000 cm^{-3} at 100 km) that are not physical. Retrieved values with a VMR below 1×10^{-10} were removed from the data prior to the error analysis and comparisons to ACE-FTS.

A. Nitric Oxide Error Calculations

The very tenuous thermosphere yields measurements with small SNR, and for this reason daily averages of SOFIE events above 80 km provide a more reliable NO measurement. The empirical precision of the NO daily averages was estimated by calculating the standard deviation of three consecutive vertical datapoints (0.6 km) in the daily average profiles. A similar calculation was done for individual events to empirically estimate the precision of a single event. A daily average includes a maximum of 15 events, so the precision of individual events should be approximately $\sqrt{15} \approx 4$ times larger. This calculation approach is an overestimation of the actual errors since it includes the natural vertical variability of NO, in addition to the random errors in the measurement. Considering that the vertical field-of-view (FOV) and the vertical resolution of the SOFIE instrument are ~1.5 and ~2.5 km, respectively, the natural variability of the datapoints contained within 0.6 km should be minimized. From these empirical calculations, the corresponding precision of the NO measurement for daily averages and individual events is shown in Fig. 6.

A daily average precision of <15% is achieved between 90 and 120 km for SR and 70 and 125 km for SS. Spacecraft SR measurements below 90 km are in general unreliable with estimated daily average measurement noise errors exceeding 20%. Many of the individual SR events are therefore not retrievable at these altitudes. This is mainly caused by the larger detector thermal oscillation, and hence larger uncertainties, for the SR mode events at lower altitudes. The daily average noise errors for both

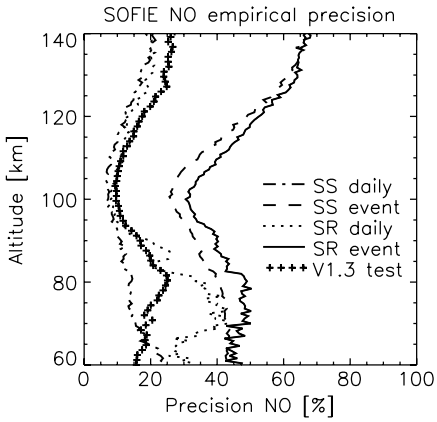

Fig. 6. NO estimated mean precision for individual events and daily averages for version V1.2. The NO precision using a retrieval with 10 interleaves is also shown as "V1.3 test."

spacecraft SR and SS gradually increase to 20% from 120 to 140 km altitude, as the NO density decreases. The empirical error calculation for individual events shows a minimum error around 100 km of ~30% and gradually increases to a maximum error of ~65% at 140 km, consistent with the diminishing signals at high altitudes. The SOFIE team is currently working on methods to improve the single event precision of the NO retrieval for the next data release. One improvement is obtained by increasing the number of interleaves used in the algorithm. The NO random error for a sample of individual SS and SR events with three additional interleaves is shown in Fig. 6 as "V1.3 test." This retrieval provides nearly the same NO precision for single events as that obtained for daily averages using Version 1.2; the trade-off, however, is a lower vertical resolution of ~3 km.

The propagation of the signal errors to the retrieved NO density was further investigated using a simulated SS NO signal. The error mechanisms considered included random noise, atmospheric temperature bias, errors in the line strengths, errors in the registration altitude, forward model uncertainties, and FOV function uncertainties. The results are summarized for an individual event in Table 1 for altitudes of 90, 120, and 140 km. An atmospheric temperature bias was simulated by applying a temperature error that linearly increased from 0 K at 60 km to 20 K at 145 km. The SOFIE temperature retrieval ends at 102 km, and the temperature above this height corresponds to the adjusted mass spectrometer incoherent scatter (MSIS) model profile [18], making temperature errors more important at high altitudes. Differences between satellite measurements and MSIS model temperature results of 40 K have been reported in the MLT region [12], making this a potential source of significant error. SOFIE data version 1.2 uses the high-resolution transmission molecular absorption database (HITRAN) 2004 [19] to simulate limb transmissions through the atmosphere. Errors in NO density are directly proportional to line strength errors, which

Table 1. Theoretical SOFIE NO VMR Retrieval Error Mechanisms for a Simulated SS Event

Error Mechanism	140 km	120 km	90 km
Random			
Signal noise (%)	40	15	10
Thermal correction (%)	15	15	6
Systematics			
FOV uncertainties (%)	2	3	4
Registration altitude (100 m) (%)	1	2	3
Temperature bias (0–20 K) (%)	8	6	5
Line strengths (7.5%) (%)	7.5	7.5	7.5
Forward model (%)	3	3	3
Total uncertainty (%)	44	24	16

were assumed to be 7.5%, following HITRAN error codes for the 5.32 μm band. The altitude registration uncertainty was simulated by applying a 100 m offset to the absorption signals before the retrieval and comparing against the retrieval with no offset. The uncertainty introduced by the correction for the detector-induced thermal oscillation was calculated empirically by retrieving on the one sigma uncertainties in the transmission signal due to the correction algorithm, as described in Section 3.B.

The empirical estimation of the error for single-event retrievals in Fig. 6 yielded higher uncertainties than the theoretical estimates. The empirical calculation is expected to be higher because of the added contribution by the geophysical variability in the measurement. However, the differences are too high to be explained entirely by geophysical variability. Notice that the theoretical calculations indicate that the bulk of the error is dominated by random errors and not systematics. This is consistent with the reduced signal at the optically thin altitudes of interest. By computing daily averages of the NO data, the random error is reduced as is the total uncertainty. When using additional interleaves ("V1.3 test" in Fig. 6), the single-event empirical errors are in better agreement with the theoretical calculations. This indicates that increasing the number of interleaves provides a more robust retrieval that produces results more in line with the theoretical error estimates in Table 1.

Another important error is the temperature bias, which would be significant at high altitudes since no actual temperature measurement is performed. However, the NO absorption measurement is directly proportional to the NO number density and relatively independent of temperature. It is only when dealing with NO mixing ratios that the temperature error will be relevant. For this reason, the NO number density is used when comparing against other satellite instruments. SOFIE and ACE-FTS measure spectral transmission, which is used to retrieve the NO number density.

B. Comparisons with Coincident ACE-FTS Events

The differing orbits of the ACE and AIM satellites limit the number of coincident measurements between the instruments. NO concentrations also

exhibit strong spatial and diurnal variations, which further constrain the extent of the coincidence window for the two satellites. For this study, the measurements were considered coincident if they occurred within 2° in latitude, 5° in longitude, and 2 h in local time. The selected window yields a total of 153 coincidences for the NH (spacecraft SR) and 144 coincidences for the SH (spacecraft SS). To perform the comparisons, the SOFIE dataset was linearly interpolated onto the ACE-FTS altitude grid. No additional smoothing of either dataset was performed in the calculations. The ACE-FTS data version 3.0 was used for the comparisons. The coincident events for the SH take place from December to April, and for the NH from March to July.

The comparisons between SOFIE and ACE-FTS NO measurements were performed between 87 and 105 km. The results are shown in Figs. 7 and 8 for the SH and NH, respectively. The mean profiles for each instrument are shown along with the difference of the mean profiles. The optically thin MLT region leads to SOFIE measurements with occasional unphysically low NO retrievals and large false variability that make individual event-to-event comparisons misleading; hence the difference of the mean profiles are shown. The plotted uncertainty for the mean SOFIE profile [panel (a) for both figures] corresponds to the daily average (15 events) precision described in Section 4.A, and represents therefore the random error in the daily average profile. The ACE-FTS uncertainty corresponds to the equivalent uncertainty for 15 event averages (mean uncertainty divided by $\sqrt{15}$). This uncertainty represents an overestimate of the actual uncertainty for the mean coincident profiles. The errors for the mean profile of the total number of coincident events will be ~3 times smaller. The total uncertainty for the difference of the means [panel (b) for both figures] corresponds to the errors of both instruments added in quadrature.

The mean SH profiles shown in Fig. 7 are almost identical for SOFIE and ACE-FTS. The total SH mean profiles differ on average by 9%. The difference range goes from −7% to 22%, except at the lower boundary where the difference is ~50%. The differences are smaller than the total estimated uncertainty at all altitudes, and most of the differences are smaller than the SEM. Note that, for clarity, the SEM in Fig. 7 is plotted at alternating altitudes for the two instruments. There is no apparent bias in the SH measurements between SOFIE and ACE.

The NH comparison in Fig. 8 shows that the coincident SOFIE NH measurements have a low bias compared to ACE-FTS. The mean SOFIE profile for the complete coincidence set was on average 18.5% smaller compared to ACE-FTS, and ranges between −33% and 11%. This result is statistically significant, as it exceeds the total uncertainty and the SEM for the differences. The difference is relatively constant throughout the comparison altitude range, except at the upper boundary, and the mean profiles from both datasets show the NO maximum at an altitude of ~99 km.

The comparisons in Figs. 7 and 8 are only shown for a limited altitude range between 87 and ~105 km because of the NO minimum between ~70 and 90 km, and because of the polar mesospheric cloud (PMC) and water interference below 85 km, which dominate the signal in this altitude range. The NO minimum and corresponding low signal in the mesosphere leads to large errors in individual measurements for both instruments. These large uncertainties prevent any comparisons throughout the NO minimum. The upper limit of the comparison is determined by the altitude at which ACE-FTS stops retrieving NO densities.

Removing SOFIE NO VMRs below 1×10^{-10}, if caused solely by random noise fluctuations in the signal, leads to an overestimation of the SOFIE NO. To evaluate this possible high bias introduced by removing the unphysical SOFIE NO VMRs, the comparison with ACE was repeated including SOFIE concentrations below the threshold. The SH results

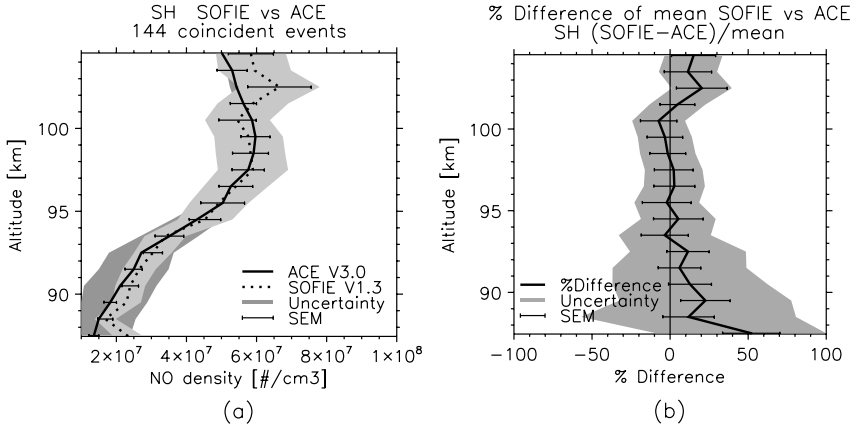

Fig. 7. NO density comparisons between SOFIE and ACE for the SH. (a) shows the mean coincident profile, the standard error of the mean (SEM) for each mean profile and the estimated daily uncertainty indicated by the shading. For clarity the SEM is plotted at alternating altitudes for the two instruments. (b) shows the difference of the mean coincident profiles, the SEM of the difference, and the total uncertainty of the two measurements.

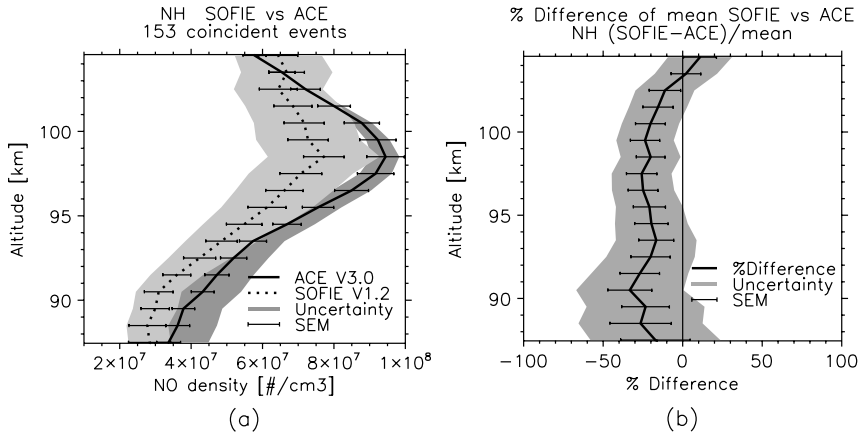

Fig. 8. NO density comparisons between SOFIE and ACE for the NH. (a) shows the mean coincident profile, the SEM for each mean profile and the estimated daily uncertainty indicated by the shading. (b) shows the difference of the mean coincident profiles, the SEM of the difference, and the total uncertainty of the two measurements.

were practically identical, with the difference between datasets still within the SEM. The difference between ACE and SOFIE for the SH becomes on average −0.85% if no removal of unphysical VMRs is performed. NH measurements show a larger difference with ACE below 93 km if all the retrieved values are included. The difference increases to −72.6% compared to −24.6%, obtained when removing the substituted VMRs. Above 93 km, the difference between ACE and SOFIE for the NH measurements changes from −15.5% to −23.6% if the unphysically low VMRs are included. The NH measurements, particularly below 93 km, are significantly sensitive to the potential systematic bias introduced by the treatment of NO VMRs below 1×10^{-10}.

To further corroborate the validity of the model throughout the altitudes of interest, a small sample of coincident ACE NO profiles (four NH and four SH events) was used to calculate the expected NO transmission for the corresponding SOFIE events. To avoid biasing the correction to the results from ACE, this analysis was done after the correction had been developed. The simulated transmission signal using the ACE NO profile was compared against the measured and corrected SOFIE signals between 87 and ∼105 km. On average, the correlation coefficient between the simulated signal and the corrected SOFIE signal was 0.61 ± 0.07. The correlation coefficient between the simulated signal and the original measured SOFIE signal was 0.37 ± 0.09, indicating that the corrected SOFIE signal best matches the simulation based on the ACE NO profile.

5. Summary and Conclusions

Thermal effects on the SOFIE NO detector have been successfully removed from the transmission signals, allowing for the retrieval of SOFIE NO densities. SH retrievals using the corrected transmission signals are currently available in SOFIE data version 1.2. The SOFIE SH retrievals are in excellent agreement with ACE-FTS coincident measurements between 87 and 105 km. SOFIE NH data show a relatively constant low bias compared to ACE-FTS of −18.5%. Efforts are underway to improve the retrieval of SR events to allow for more accurate NH measurements.

A challenge in the retrieval of thermospheric NO is the extremely optically thin atmosphere above 90 km, yielding small absorption signals. To obtain improved SNR, several event averages were used. Daily average measurements (15 events) have an empirically estimated error of <15% at altitudes between 90 and 120 km for both hemispheres. Future SOFIE data versions will study the implementation of algorithm improvements that reduce the retrieval random error to ∼25% for individual events from 60 to 130 km, in agreement with theoretical error calculations.

The SOFIE NO dataset for the SH has been restored to scientific quality, despite the detector thermal response nonlinearities. The NH measurements are still under study, but also show improved NO density profiles. This initial validation will be expanded in a future study to include other NO measurements. The relatively good agreement with ACE-FTS for both hemispheres is a good indicator of the reliability of current SOFIE NO retrievals above 87 km.

Funding of the AIM mission was provided by NASA's Small Explorers Program under the contract NAS5-03132. The Atmospheric Chemistry Experiment (ACE), also known as SCISAT, is a Canadian-led mission mainly supported by the Canadian Space Agency and the Natural Sciences and Engineering Research Council of Canada.

References

1. C. Barth, K. Mankoff, S. Bailey, and S. Solomon, "Global observations of nitric oxide in the thermosphere," J. Geophys. Res. **108(A1)**, 1027–1037 (2003).
2. S. M. Bailey, C. A. Barth, and S. C. Solomon, "A model of nitric oxide in the lower thermosphere," J. Geophys. Res. **107(A8)**, SIA 22 (2002).
3. C. Randall, V. Harvey, C. Singleton, P. Bernath, C. Boone, and J. Kozyra, "Enhanced NO_x in 2006 linked to strong upper

stratospheric arctic vortex," Geophys. Res. Lett. **33**, L18811 (2006).
4. C. E. Randall, V. L. Harvey, G. L. Manney, Y. Orsolini, M. Codrescu, C. Sioris, S. Brohede, C. S. Haley, L. L. Gordley, J. M. Zawodny, and J. M. Russell III, "Stratospheric effects of energetic particle precipitation in 2003–2004," Geophys. Res. Lett. **32**, L05802 (2005).
5. D. Siskind, G. Nedoluha, C. Randall, M. Fromm, and J. M. Russell III, "An assessment of southern hemisphere stratospheric NO_x enhancements due to transport from the upper atmosphere," Geophys. Res. Lett. **27**, 329–332 (2000).
6. M. G. Mlynczak, L. A. Hunt, B. T. Marshall, F. J. Martin-Torres, C. J. Mertens, J. M. Russell III, E. E. Remsberg, M. Lopez-Puertas, R. Picard, J. Winick, P. Wintersteiner, R. E. Thompson, and L. L. Gordley, "Observations of infrared radiative cooling in the thermosphere on daily to multiyear timescales from the TIMED/SABER instrument," J. Geophys. Res. **115**, A03309 (2010).
7. L. L. Gordley, M. E. Hervig, C. Fish, J. M. Russell III, S. M. Bailey, J. Cook, S. Hansen, A. Shumway, G. Paxton, L. Deaver, T. Marshall, J. Burton, B. Magill, C. Brown, E. Thompson, and J. Kemp, "The solar occultation for ice experiment (SOFIE)," J. Atmos. Sol. Terr. Phys. **71**, 300–315 (2009).
8. P. Bernath, C. McElroy, M. Abrams, C. Boone, M. Butler, C. Camy-Peyret, M. Carleer, C. Clerbaux, P.-F. Coheur, R. Colin, P. DeCola, M. DeMazière, J. R. Drummond, D. Dufour, W. Evans, H. Fast, D. Fussen, K. Gilbert, D. Jennings, E. Llewellyn, R. Lowe, E. Mahieu, J. McConnell, M. McHugh, S. McLeod, R. Michaud, C. Midwinter, R. Nassar, F. Nichitiu, C. Nowlan, C. Rinsland, Y. Rochon, N. Rowlands, K. Semeniuk, P. Simon, R. Skelton, J. Sloan, M.-A. Soucy, K. Strong, P. Tremblay, D. Turnbull, K. Walker, I. Walkty, D. Wardle, V. Wehrle, R. Zander, and J. Zou, "Atmospheric chemistry experiment (ACE): mission overview," Geophys. Res. Lett. **32**, L15S01 (2005).
9. C. D. Boone, R. Nassar, K. A. Walker, Y. Rochon, S. D. McLeod, C. P. Rinsland, and P. F. Bernath, "Retrievals for the atmospheric chemistry Experiment Fourier-transform spectrometer," Appl. Opt. **44**, 7218–7231 (2005).
10. P. Sheese, R. Gattinger, E. Llewellyn, C. Boone, and K. Strong, "Nightime nitric oxide densities in the southern hemisphere mesosphere-lower thermosphere," Geophys. Res. Lett. **38**, L15812 (2011).
11. R. L. Gattinger, I. C. McDade, A. L. A. Suzán, C. D. Boone, K. A. Walker, P. F. Bernath, W. F. J. Evans, D. A. Degenstein, J.-H. Yee, P. Sheese, and E. J. Llewellyn, "NO_2 air afterglow and O and NO densities from ODIN-OSIRIS night and ACE-FTS sunset observations in the antarctic MLT region," J. Geophys. Res. **115**, D12301 (2010).
12. D. Bermejo-Pantaleón, B. Funke, M. López-Puertas, M. García-Comas, G. P. Stiller, T. von Clarmann, A. Linden, U. Grabowski, M. Höpfner, M. Kiefer, N. Glatthor, S. Kellmann, and G. Lu, "Global observations of thermospheric temperature and nitric oxide from MIPAS spectra at 5.3 μm," J. Geophys. Res. **116**, A10313 (2011).
13. H. Bovensmann, J. P. Burrows, M. Buchwitz, J. Frerick, S. Noel, V. V. Rozanov, K. V. Chance, and A. P. H. Goede, "SCIAMACHY: mission objectives and measurement modes," J. Atmos. Sci. **56**, 127–150 (1999).
14. J. M. Russell III, S. M. Bailey, M. Hornyi, L. L. Gordley, D. W. Rusch, M. E. Hervig, G. E. Thomas, C. E. Randall, D. E. Siskind, M. H. Stevens, M. E. Summers, M. I. Taylor, C. R. Englert, P. Espy, W. E. McClintock, and A. W. Merkel, "Aeronomy of ice in the mesosphere (AIM): overview and early science results," J. Atmos. Sol. Terr. Phys. **71**, 289–299 (2009).
15. R. J. Sica, M. R. M. Izawa, K. A. Walker, C. Boone, S. V. Petelina, P. S. Argall, P. Bernath, G. B. Burns, V. Catoire, R. L. Collins, W. H. Daffer, C. De Clercq, Z. Y. Fan, B. J. Firanski, W. J. R. French, P. Gerard, M. Gerding, J. Granville, J. L. Innis, P. Keckhut, T. Kerzenmacher, A. R. Klekociuk, E. Kyrö, J. C. Lambert, E. J. Llewellyn, G. L. Manney, I. S. McDermid, K. Mizutani, Y. Murayama, C. Piccolo, P. Raspollini, M. Ridolfi, C. Robert, W. Steinbrecht, K. B. Strawbridge, K. Strong, R. Stübi, and B. Thurairajah, "Validation of NO_2 and NO from the atmospheric chemistry experiment (ACE)," Atmos. Chem. Phys. **8**, 5801–5841 (2008).
16. J. Mor, "The Levenberg-Marquardt algorithm: implementation and theory," in *Numerical Analysis*, G. Watson, ed. Vol. 630 of Lecture Notes in Mathematics (Springer, 1978), pp. 105–116.
17. J. M. Russell III and S. R. Drayson, "The inference of atmospheric ozone using satellite horizon measurements in the 1042 cm^{-1} band," J. Atmos. Sci. **29**, 376–390 (1972).
18. J. Picone, A. Hedin, D. Drob, and A. Aikin, "NRLMSISE-00 empirical model of the atmosphere: statistical comparisons and scientific issues," J. Geophys. Res. **107**, 1468–1483 (2002).
19. L. Rothman, D. Jacquemart, A. Barbe, D. C. Benner, M. Birk, L. Brown, M. Carleer, C. Chackerian, K. Chance, L. Coudert, V. Dana, V. Devi, J.-M. Flaud, R. Gamache, A. Goldman, J.-M. Hartman, K. Jucks, A. Maki, J.-Y. Mandin, S. Massie, J. Orphal, A. Perrin, C. Rinsland, M. Smith, J. Tennyson, R. Tolchenov, R. Toth, J. V. Auwera, P. Varanasi, and G. Wagner, "The HITRAN 2004 molecular spectroscopic database," J. Quant. Spectrosc. Radiat. Transfer **96**, 139–204 (2005).